

RESEARCH ARTICLE

Open Access



Measuring impacts of microplastic treatments via image recognition on immobilised particles below 100 µm

Robin Lenz^{1*} , Kristina Enders¹, Franziska Fischer², Josef Brandt³, Dieter Fischer² and Matthias Labrenz^{1*}

Abstract

The treatment of samples for microplastic (MP) analysis requires purification steps that sufficiently reduce the non-MP content while preserving the targeted particles integrity. Besides their macromolecular structure this also encompasses their in situ numbers and sizes. However, any step of sample manipulation will come at a cost: particle loss, fragmentation, coagulation or degradation may lead to distorted results, predominantly in the smaller fraction of the MP size range. Therefore, the evaluation of MP resistivity against applied methods such as chemical digestions is a vital criterion for obtaining meaningful results on MP content of a sample. We developed a framework to test the applicability of MP purification methods and apply it to four protocols commonly used to prepare environmental samples for MP particle identification. The approach was designed for MP particles being too small to be handled manually (i.e. 10–70 µm). The evaluation consists of a two-tiered assay: a simple particle suspension approach is used to confirm a post-treatment qualitative recognisability of the target polymers by the analysis method of choice (here Raman and FTIR). In a following quantitative part, immobilised particles are used to evaluate the preservation of particle numbers and areas after the treatment on an individual particle level. A Python image analysis package was written that identifies, matches and measures particles on pairs of pre- and post-treatment images, and is available as open source software. Our results show that the chemical digestions using hydrogen peroxide, cooled Fenton's and a combined alkaline / oxidative treatment using potassium hydroxide and sodium hypochlorite are suitable methods for preparing MP samples for a microspectroscopic analyses. Also acidic sodium polytungstate solution used for MP density separations and a pentane based protocol for lipid removal were found applicable for small sized MP. Certain degradative effects were found when acrylonitrile butadiene styrene is exposed to acidic treatments, as well as for MP from acrylate and epoxy based paint resins in strong oxidative regimes. Several paint resins tested here were spectroscopically not identifiable by polymer attributed bands even before treatment, indicating that these materials might slip through analyses of environmental samples and consequently being underreported. We conclude that evaluating chemical treatment procedures on MP < 100 µm is feasible, despite limitations of the current methodology which we discuss. Our results provide more certainty on the tested methods for MP studies specifically targeting small sizes and should be extended for more protocols used in MP laboratory practises.

Keywords: Microplastics, Purification, Digestion, Qualitative, Quantitative, Resistivity, Method evaluation, Validation, Image recognition

* Correspondence: robin.lenz@io-warnemuende.de; matthias.labrenz@io-warnemuende.de

¹Leibniz Institute for Baltic Sea Research Warnemünde, Seestraße 15, 18119 Rostock, Germany
Full list of author information is available at the end of the article

Introduction

Microplastic (MP) purification techniques were developed by a number of studies in order to facilitate measurements of abundance of this inhomogeneous group of environmental contaminants [1–12] and reviews of recent developments are available [13–18]. Within MP, practically any synthetic polymeric material can be of interest, among others classical thermoplastics, varieties of elastomers as well as paint resins. The challenge has been to extract all relevant particles from the large diversity of sample matrices.

Depending on the system studied these matrices typically consist to large degrees of inorganic fractions like minerals from sediments and soils [19], and organic content such as detritus, tissue or microbial films, particularly confounding spectroscopic analysis [20]. The contained MP loads often range in the ppm to ppt (w/w, [21]). Physical density and chemical inertness to certain degradative agents are the two most harnessed properties of MP to facilitate a separation from the respective sample matrix. However, both of these principles involve deficiencies contributing to uncertainties in the resulting numbers or masses of MP obtained through the subsequent analysis of the treated samples.

For density separation, hydrodynamic problems occur that can hinder the intended particle advection. These include flocculation or coagulation of targeted and non-targeted particles altering the apparent density [22] as well as forces such as turbulence and adhesion [23] counteracting the — with decreasing particle size diminishing — impact of buoyancy. Also mechanical action involved in any extraction technique can contribute to errors for instance if samples are incompletely transferred between vessels or particles are altered through activities such as shaking, grinding, stirring or ultrasonication [24]. In chemical digestion processes loss of relevant particles can occur through unwanted chemical interactions of certain MP species with the applied digestant such as oxidation, hydrolytic polymer chain cleavage, or bleaching.

Purification steps aiming at the removal of non-targeted material through dissolution involve chemicals that exhibit degradative effects on these materials while — in the optimal case — leaving the present MP unimpacted. Based on the high chemical diversity of both, the material group of plastics and the unwanted constituents, the selection of suitable protocols for purification are a critical and difficult task. This includes the rigorous testing of the MP particles resistivity to a method in question. A broad range of plastic polymer types needs to be examined, as their large chemical diversity provides a variety of possibilities for chemical degradation. The size range of particles being tested needs to match the lower sizes of MP targeted by the planned

environmental studies aiming to apply the respective protocol. Existing method development and validation studies often tested against larger MP or macroplastic items [1, 25, 26], which allows relatively simple experimental designs. The resistance of larger plastic objects (e.g. millimetre sized pellets) against a digestive reagent is, however, no sufficient cause to assume that this would be equally the case for MP orders of magnitude smaller. Hence, MP particles in the lower μm size are of paramount importance in method validation tests, which was also emphasised by another recent study [12]. There are reasons to attest them a higher vulnerability to chemical degradation than larger particles, due to their increased surface to volume ratio, resulting in a higher number of exposed polymer backbones, functional groups and chain ends. Furthermore, the polymer matrices of MP particles in the lower micrometre scale are not necessarily homogenous, even when coming from the same origin. In the environment, weathering may reach individual particles differently and therefore produce varieties of particles differing in mean molecular weight and prevalent functional groups as well as end groups. The shares of crystalline and amorphous domains (i.e. regions of different chain folding and conformation) are related to vulnerability to degradation [27] and the typical domain size depends on the molecular weight of the chain fragment [28]. In semi-crystalline polymers the sizes, numbers and shapes of MP formed in fragmentation of degrading macroplastics depend on their crystalline morphology [29]. Varying additive content also influences certain polymer properties like mechanical strength or oxidative resistance [30].

Aim and scope

The scope of the present study is to evaluate the resistance of MP against chosen chemical agents on the example of treatment protocols previously recommended for purification of MP samples (as summarised by Enders et al. [31]). As stated above, there is already an extensive knowledge base in the literature on a variety of treatment methods, although rather heterogeneous. There is a knowledge gap, however, for resistivity of particles in the lower μm sizes, including a lack of methods for manipulations and measurements on an individual particle basis and simultaneously in large numbers. The endpoint of evaluation hereby should be the qualitative and quantitative detectability of the treated MP by microspectroscopic analyses and microscopic imaging. Our contribution is to study the impact of protocols including oxidative, alkaline, acidic and organic solvent based chemicals. They are tested on 19 polymer types (including 5 synthetic paint resins) in the size range of 10 to 70 μm (Table 1). Our primary objective is to enable method testing for particles below 100 μm , which

Table 1 Specifications of test MP particles, ^a rosin may not be regarded as a polymeric resin matrix, but was included as it is a common ingredient in self-eroding antifouling coatings of ships, and may therefore be a relevant type of environmental paint flakes

Group	Sample Name	Long Name	Origin (product name and manufacturer)	Colour	Density
Commodity Plastics	ABS	acrylonitrile butadiene styrene	Terluran GP-22, Ineos Styrolution	white	1.04
	EVA	ethylene vinyl acetate	Escorene Ultra FL 00328, Exxon Mobil	white	0.951
	HDPE	high density polyethylene	HDPE HTA 108, Exxon Mobil	white	0.961
	LDPE	low density polyethylene	LDPE LD 100.BW, Exxon Mobil	white	0.923
	PA6	polyamide 6	Ultramid B40, BASF	white	1.14
	PA6.6	polyamide 6.6	Ultramid A34 01, BASF	white	1.13
	PA12	polyamide 12	Vestamid L1600, Evonik	white	1.01
	PC	polycarbonate	Lexan 121R, Sabic	white	1.2
	PET	polyethylene terephthalate	ES306030/1 powder, Goodfellow	white	1.3–1.4
	PMMA	polymethyl methacrylate	Plexiglas 8N, Evonik	white	1.19
	PP	polypropylene	Moplen HP400R, LyondellBasell	white	0.9
	PS	polystyrene	Polystyrol 143 E, BASF	white	1.043
	PVC	polyvinylchloride	EVIPOLE SH6830, Globichem	white	~ 1.4
	TPU	thermoplastic polyurethane	Elastollan C85A10, BASF	white	1.19
Paint resins	rosin ^a	maritime antifouling rosin resin	Hempel's Classic 76110, Hempel	red	n/a
	acrylate	general purpose primer acrylic resin	b1, J.W. Ostendorf	white	n/a
	PU	anticorrosive polyurethane resin	Temadur SC 533, Tikkurila Oyj	black	n/a
	epoxy	maritime anticorrosive epoxy resin	Hempadur 45148, Hempel	red	n/a
	alkyd	maritime primer alkyd resin	Hempel's Underwater Primer 26030, Hempel	grey	n/a

cannot easily be handled or manipulated due to their small size. A description of where the scope of this study has its boundaries is detailed further in the SI (S1).

We evaluate polymer resistivity to each protocol based on the following two questions:

- Qualitative: Are there diminishing effects on the spectroscopic recognisability of the polymer?
- Quantitative: Are sizes or particle numbers significantly altered?

Besides the reporting of the tested resistivities, this study commits to the principles of the open science approach, wherefore underlying data and procedures, including all implementations of algorithms that were developed in this study, are made publicly available.

Comparison of our concept to other approaches in current literature

Several studies reported polymer resistivity based on particle recoveries in spiked real matter matrices (e.g. sediments [10], soil and sludge [32, 33], or biota [10, 11]). This allows combining the evaluation of the efficacy of a digestion (matrix reduction) and the possible effect on the MP particles. However, also interactions between the matrix and MP particles may occur and can obfuscate the effects of the treatment itself on the polymers.

While this may be regarded as being more realistic with respect to an actual environmental MP purification, it is less comparable and generalisable. The influence of matrix parameters (e.g. grain size, material composition) and the interaction with the spiked MP particles (coagulation, grinding, etc.) during purification treatments are not yet well understood [31]. When the focus is primarily on effects of the treatment on the polymer, the combination of digestion efficiency and polymer resistivity tests is not compulsory to yield insight into effects individual treatments may have on certain polymer particles. We chose to operate in a matrix-free environment, as to gain primary insight into the genuine reagents-particles-interactions, but acknowledge that these treatments would only practically be used in the presence of a matrix, that must be reduced, as this is the primary goal of these treatments. Hence, our assessments can be valuable basis for future matrix-specific treatment validations, which are an important and logical next step.

Evaluation tests could be done without a matrix solely by applying the treatment to a particle suspension. The post-treatment state may then be measured by solid state technique, e.g. microscopic imaging after an additional filtration step, or by liquid phase techniques such as Beckman-Coulter-Counters, flow-cytometry, laser diffraction or dynamic image analysis. Each of these techniques will have their own advantages and limitations,

but commonly, it can be said that the experimental setup and conduction would be comparably simple, as the techniques are well established, and large particle amounts could be measured (for microscopic imaging with the constraint of required filter area and measuring time). It is however not possible to relate the post-treatment measurements directly to the pre-treatment state of the same particle. When measuring effects on median particle sizes or similar properties, this is of little relevance when the particle number is large enough to yield meaningful statistical aggregates. Particle counts and their treatment-induced changes, are, however, not readily inferred from suspended bulk measurements. Furthermore, approaches working with mobile particles are prone to errors owed to the manual handling of the particles (e.g. filtration, rinsing), which are difficult to account for when working with small MP. Here lies the prospect of the technique used in the present study, where MP particles are immobilised on a plane surface, and microscopic measurements of individual particles can be linked between pre- and post-treatment conditions.

General background on the experimental model design

To evaluate the applicability of MP treatment protocols, we expose the test material of irregularly shaped MP particles to the chemicals and physical conditions of the respective protocol (Fig. 1). Before and after exposure we take the measurements on those particles as detailed below.

In a typical MP particle-based analysis the particle material is first qualitatively determined (e.g. spectroscopically, to decide acceptance or rejection as MP) and, second, for confirmed MP further properties are obtained optically (e.g. size, colour, shape). For our method validation concept, we formalised those distinct categories of measurements as two separate experimental approaches that are each optimised for their respective requirements.

Using qualitative measurements, i.e. Raman and Fourier transform infrared (FTIR) spectra, we need to determine whether a reagent has reacted with a polymer to a degree that it would no longer be recognised as what it is by means of its spectroscopic signal. To obtain this information it is not necessary to handle individual particles, which is difficult and time demanding in the targeted size range. Instead, here it is sufficient to work with bulk particle suspensions. An approximate amount of test particles is added to the liquid reagent and removed after the treatment period is over. A complete recovery of particles is not necessary. Spectra can then be acquired on any of the recovered particles. However, qualitative measurements alone are insufficient to evaluate a protocol's applicability. We need to assume that fractions of particles could be destroyed by the treatment, while others persisted and could be measured.

Quantitative measurements allow us to make a statement on whether and to which degree particles have been lost or deformed during the treatment. Due to the chosen size range individual handling of particles (e.g. by

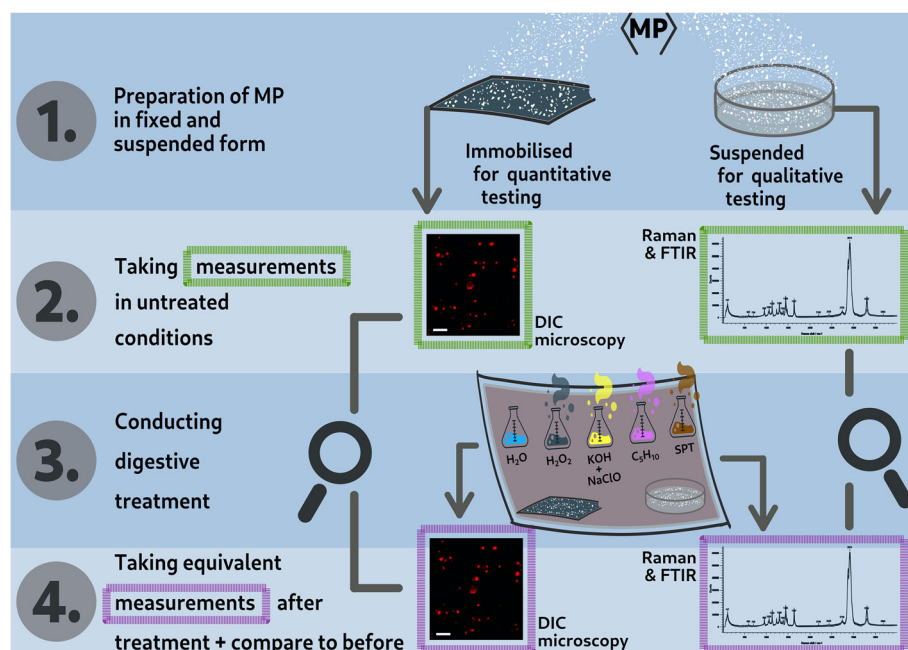


Fig. 1 Schematic visualisation of the method validation concept in a qualitative and a quantitative workflow

tweezers) for transfer or counting, is no suitable approach here. At the same time, large numbers of particles should be processed to allow for a robust statistical analysis of the measurements. The here presented approach is based on immobilising the MP particles on a silicon wafer coated with a thin film of epoxy resin. This method allows us to compare pre- and post-measurements on an individual particle basis which enables a more granular analysis, e.g. with respect to differences across the particle size spectrum. A microscopic image of a defined region of the wafer serves as the pre-treatment data point and is compared to an image of the exact same region after the treatment has been conducted.

It should be noted here that this combination of a qualitative and quantitative approach will not be able to pick up qualitative-only effects (i.e. chemical alterations not leading to effects on the quantitative particle properties), that do not occur in all particles of a polymer in a specific treatment, but rather only a hypothetical minority with certain characteristics. By the nature of the particles used herein - all being produced in the same manner from pristine raw materials - such deviant behaviours are not assumed to be occurring relevant numbers. It would be, however, a question worth investigating for future studies aiming at particle stability during treatments with a more detailed focus on exact particle properties, such as very narrow size and shape ranges, or specific surface properties.

Methods

Preparation of polymer test materials

For the group of commodity plastics pre-production polymer pellets were cryo-milled and sieved to yield particles of the targeted size range. The raw materials of

each polymer type (see Table 1), were individually submitted to cryogenic ball milling (Retsch CryoMill, 50 ml grinding jar, 25 mm ball, 5–6 g raw material, pre-cooling: 10 min at 5 Hz, 6 grinding cycles consisting of 2 min milling at 35 Hz and 2 min cooling at 5 Hz). The fraction that was used in the following procedures consisted of particles that passed a 71 µm, but were retained on a 10 µm stainless steel analytical sieve (Topas GmbH). The group of paint resin polymers was obtained from commercial consumer or industrial products of common outdoor appliances or maritime paints, which were tempered as recommended by the manufacturers and squeegeed in customary manner. Films were left to cure and later ground and sieved as described above by cryo-milling.

Treatment specifications

The specifications were adapted from the original protocol references and are detailed in Table 2. All treatment solutions were filtrated at 1.5 µm prior to application (vacuum filtration in glass bottles, Whatman 943-AH glass filter membranes) and 3–5 ml of the respective reagent were added to ensure that all MP particles were wetted.

In contrast to all other treatments, the H₂O₂ treatments were not consistent between the qualitative and the quantitative analyses. Qualitatively we tested Fenton's catalysed H₂O₂ digestions (cooled and uncooled), as well as a non-catalysed 2 weeks long exposure. The quantitative approach did not include Fenton's catalysed reactions. The strongly exothermic progression of Fenton's reactions were regarded as a practically not feasible application for the particle immobilisations: strong heat and foam formation would hinder an equal exposure of all particles on a wafer. Also the 2 weeks long exposure

Table 2 Short specifications and protocol references to the tested treatments

Treatment name	Specifications	Protocol Reference
Water (negative control)	ultra-purified water, 24 h, RT	–
H ₂ O ₂ Fenton's (Fe) uncooled ^a	30% H ₂ O ₂ + catalyst (6.67 mg ml ⁻¹ of Fe(II)SO ₄ , pH 4), ca. 10 min, max. 85 °C (measured after 5 min)	[2]
H ₂ O ₂ Fenton's (Fe) cooled ^a	30% H ₂ O ₂ + catalyst (6.67 mg ml ⁻¹ of Fe(II)SO ₄ , pH 4), 24 h, 20–30 °C (on ice, measured after 5 min)	[2]
H ₂ O ₂ LT ^a	30% H ₂ O ₂ , non-catalysed, 14 days, RT	[31]
H ₂ O ₂ ^b	30% H ₂ O ₂ , non-catalysed, 24 h, RT	[31]
KOH + NaClO	per 1 L: 700 ml H ₂ O, 150 ml NaClO 14% active chlorine and 150 ml saturated KOH (1120 g L ⁻¹), 5 h, RT	[1]
Pentane (C ₅ H ₁₀)	15 min in an immiscible water - ethanol (pH 3) - pentane mixture (5:1:1), shaken 3 times, 30–35 °C	[31]
SPT	Sodium polytungstate solution 1800 kg m ⁻³ , acidified with HCl (pH 3), 24 h, RT	[31]
HCl (positive control) ^b	one wafer with PA6, only for image processing algorithm calibration: 10% HCl, 20 min, RT, to fully dissolve MP	–

RT room temperature, LT Long term

^a only in qualitative part, ^b only in quantitative part

to non-catalysed H_2O_2 was replaced by a 24 h period, as it was uncertain whether the epoxy adhesive layer would withstand the 2 weeks exposure to a degree necessary to uphold its function of immobilising the particles. For many MP sample purifications scenarios this still resembles a typical application duration, i.e. for water samples [31]. The longer treatment in the qualitative part could be regarded to cover any effects that would also occur in the 24 h quantitative measurements, but not necessarily vice versa. This should be kept in mind when drawing detailed conclusions from the here presented data on the specific treatment protocols.

Qualitative analysis

Preparation and spectra acquisition

Prior to treatment, FTIR and Raman spectra were obtained on the milled test-MP particles as a spectroscopic reference. Approximately 5 mg of each of these particles were submitted to the respective treatments (Table 2). After the treatment procedure was completed, the particles were retained in a wet filtration on a vacuum filtration device with a stainless steel sieve of 10 μm nominal pore size (Spörl KG). On the filter, the particles were thoroughly rinsed with MP-free H_2O (prepared according to Enders et al. [31]) before few particles were manually transferred to a Si wafer as a plane spectroscopic substrate. Post-treatment spectroscopy was conducted using ATR-FTIR (PerkinElmer Spotlight 400, spectral resolution: 4 cm^{-1} , 32 scans, or Bruker ATR microscope Hyperion 2000 with 20x ATR objective, coupled to Bruker FTIR spectrometer Vertex 70, spectral resolution: 4 cm^{-1} , 100 scans) and Raman microscopy (Renishaw, inVia Qontor, laser: 532 nm, 100 accumulations, 0.5 s per scan, magnification: 50x, laser power: 60 μW - 4 mW). The settings used for each instrument were manually chosen to provide a sufficient spectroscopic data quality that allowed for the intended analyses and conclusions to be drawn. Which spectra were measured on which instrument and settings may be inferred from the deposited spectra data set [34], where the name of the spectrometer is given for each spectrum measured. For each treatment and polymer, three different MP particles were spectroscopically analysed as replicates as a minimum.

Data analysis

To compare and evaluate the Raman spectra, all replicates of one treatment and a representative spectrum of the untreated material (reference) were plotted together using the Renishaw WiRE 5.2 software. Changes, such as baseline shifts or the occurrence of new peaks were noted. For spectra with newly emerged peaks, a library search was conducted using the WITec TrueMatch 5.2 software. We searched the range of 200 to 4000 cm^{-1}

after a shape background subtraction was applied (subtract shape size: 200). The hit quality index (HQI) was then calculated as the Pearson Correlation Coefficient of the non-derivative spectra. The commercially available ST Japan Raman libraries for pristine polymer references were used. For the FTIR spectra, reference and treatment-specific spectra were plotted in the same way using either the Perkin Elmer Spectrum software or the Bruker OPUS (v7.5) software and changes were noted. Manual spectra evaluation was used to detect any changes in molecular vibration frequencies and to suggest their origin. For example, the emergence of new IR bands in the range of 1580–1600 cm^{-1} and 1350–1380 cm^{-1} indicates generation of a carboxylic acid salt as a result of polymer oxidation. The FTIR spectroscopic evaluations included also the calculation of HQIs, which were performed to assist in the manual spectra evaluation, but were deliberately not used as the sole decision criterion. Their calculation was conducted in the Bruker OPUS software using the proprietary Euclidean-distance-based HQI algorithm and the following list of libraries: ATR-LIB-COMplete Vol 1–3 (ST Japan), Hummel Industrial Polymers (Chemical Concepts), Hummel (Bruker), MERCK (Bruker), Polymer library (Bruker), General library IR (Bruker) and a custom library of self-measured common polymer types.

To classify changes in the spectroscopic signals, we assigned each treated polymer to one of four categories (Table 3). The decision on a category was derived as the result of the manual spectra evaluation as described above. Where replicates exhibited different changes in spectra, the decision was based on what the majority of replicates indicated. We defined the categories with the goal to differentiate the spectra into groups of similar chances for successful spectroscopic polymer recognition. Similar categorisation approaches have been taken by other MP treatment validation studies [1, 14]. Category “x” was assigned when an evaluation could not be conducted, because, independent of treatment, no exploitable spectral bands spawned from the respective polymer with the respective spectroscopic technique.

When identifying environmental MP spectroscopically, usually semi-automated library searches are used instead of manual spectra evaluations. For a subset of the polymer types, we reported Raman HQI values of the highest correct polymer type match and compared deviations between the reference HQI (untreated polymer) and HQI of treated replicates with our manual category assignments.

Quantitative analysis

Based on the qualitative test and previously published resistance studies, a set of polymers and treatments was selected for further quantitative analysis. The decision to

Table 3 Categories used to evaluate the impact of a treatment on the spectroscopic recognisability of the treated polymers. Exemplary spectra for each category can be found at the given page numbers in the respective data deposits: ^a Raman+FTIR_commodityPolymers.pdf, ^b Raman+FTIR_paintResins.pdf

Category	Definition	Consequences	Example Spectra Raman	Example Spectra FTIR
0	no relevant changes, spectra identical within natural background noise levels	polymer recognition unhindered	p. 77 in [34] ^a	p. 156 in [34] ^a
1	changes in non-band spectral properties, i.e. baseline slope or elevation, fluorescence	polymer recognition unhindered, changes do not mask polymer bands	p. 44 in [34] ^a	n/a
2	emergence of new bands or individual band intensities increased due to polymer degradation processes (e.g. oxidation)	polymer recognition largely unhindered, changes do not mask polymer bands	p. 23 in [34] ^b	p. 11 in [34] ^a
3	removal or strong alteration of polymer specific bands	polymer recognition is hindered	p. 20 in [34] ^b	n/a
x	no polymer specific spectrum measurable independent of treatment	no evaluation possible	p. 31 in [34] ^b	p. 41 in [34] ^b

not analyse all polymers that were included in the qualitative part was due to the limited analytical capacities. Of chemically similar polymer types only one representative was used (polyethylenes and polyamides). In the group of paint resins, we limited the selection to the acrylate and epoxy based products, of which we got usable results in the qualitative part of the study.

Preparation of particle immobilisations

For the quantitative analysis particles were immobilised on silicon wafers with a thin epoxy resin layer as an adhesive (see Fig. 2). Rectangular pieces, ca. 1–2 cm², 700 µm thick, were cut from the silicon wafer material and initially cleaned by being immersed and rotated for at least 10 min in piranha solution (H₂SO₄ 60% and H₂O₂ 30% mixed in a 1:1 ratio just before the wafers were added). The cleaned wafers were coated with a layer of epoxy resin (L20 + EPH 161 thinned with acetone, 100:25:25 weighed ratio, Hex-ion). The resin has a drip time of 90 min. A single wafer piece was mounted on a spin coater chuck and

spun at 7500 rpm for approximately 20 s (Polos BL MCD, APT GmbH, Germany). The film thickness was determined via z-axis differences for focus on the wafer surface versus focus on the film surface using the same instrument and settings as described below (Image acquisition and reagent application). On eight random locations the mean thickness was 4.25 µm with a standard deviation of 1.98. After a short curing interval of approximately 2 min, the test-MP of one polymer type were applied to the glue surface by trickling them through a stainless steel mesh (100 µm pore size, held approximately 5 cm above the wafer) with help of a metal spatula. The particles came to rest on the still adhesive resin layer and the wafer was left at 40 °C to fully cure overnight. For each treatment, one wafer per polymer was prepared in this way. During spin coating and particle application the wafers were only handled inside a ventilated cabinet and were placed in closed-lid transparent polystyrene boxes for transport and curing, as to prevent unintended dust particle settling.

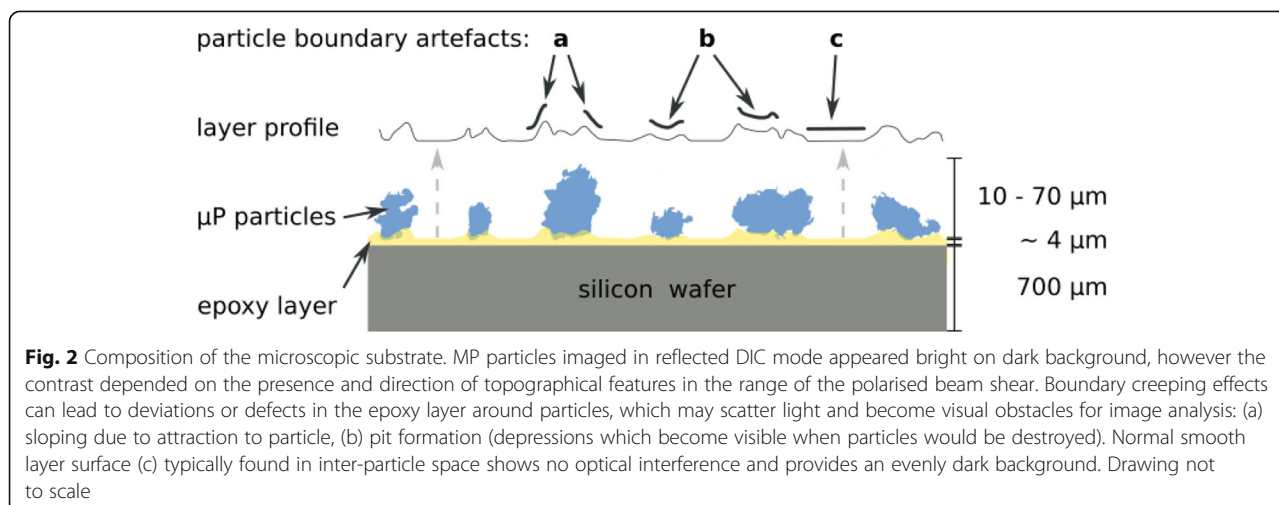


Image acquisition and reagent application

Optical microscopic images were acquired with a Zeiss Axio Imager.Z2m digital microscope on a defined region of each coated wafer (prior to treatment) after they had been rinsed with ultra-purified H₂O and dried with nitrogen purge gas to remove any loose particles or dust. Each wafer was then exposed to one of the treatment reagents (see Table 2) and rinsed again with ultra-purified H₂O to remove any residual chemical reagents. A post-treatment image was then obtained from the same area on the wafer as for the pre-treatment image. All images were taken using the Zeiss Zen software v2.7, a 20 x objective in reflected light differential interference contrast (DIC) mode. DIC was chosen as it gave the largest contrast difference between particles and background, when compared with other techniques (bright field and dark field). The resulting image signal-to-noise ratio depended however strongly on the polymer type, limiting the applicability of this technique for some polymers (i.e. PVC and PMMA, see also section Methodological caveats for an evaluation of diagnostic limitations). Images were acquired as tiling mosaics with a fixed zero overlap stitching. It was necessary to postprocess the images manually. For pairs of corresponding pre- and post-treatment images areas of visual artefacts (e.g. air entrainment on wafer borders) were cropped simultaneously (Fig. 3 shows the differences between original and

processed images). Differing light conditions in the original images were accounted for by histogram adaptation (conducted equally for pre- and post-image pairs). The images used for analysis were in 8-bit tiff format with a pixel resolution of 0.72 $\mu\text{m px}^{-1}$.

Image analysis

Particle identification algorithm The analysis routine for the DIC images was written in python and is available for use and contribution under GNU GPL v3.0 at: https://github.com/robna/ImmobileParticles_MatchAndAnalyse, and as a static citable version [35]. A number of open source python libraries were used, most notably: Altair [36] which builds on the declarative visualisation grammar Vega-Lite [37], pandas [38, 39], statsmodels [40], OpenCV [41] and SKimage [42]. The routine consists of a three-step procedure (Table 4).

First, a particle recognition routine identifies particles on both the pre- and the post-treatment image. Their coordinates are used to align the images, i.e., to remove any image tilt and offset. From the aligned images, for each particle in the pre-treatment image the corresponding particle in the post-treatment image is identified (if present). This particle matching allows determining and comparing particle statistics, such as size or brightness, before and after the treatment on a per-particle basis.

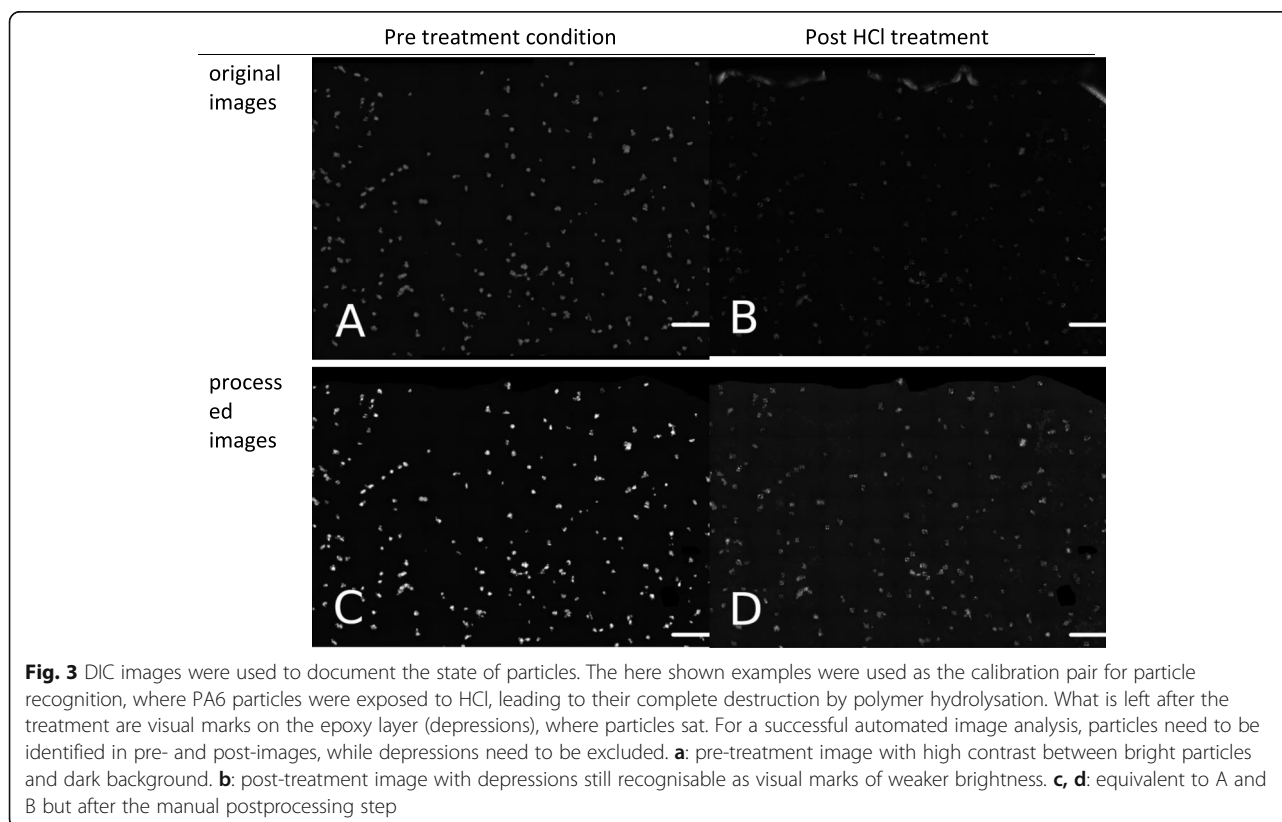
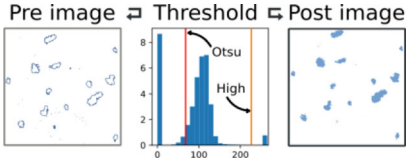
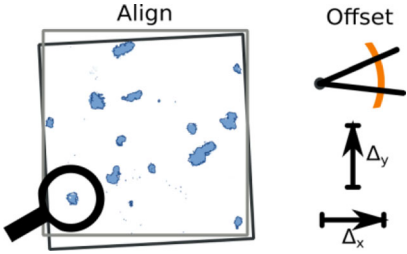
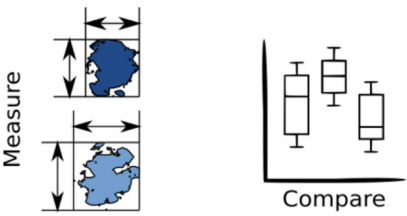


Table 4 Steps of the image analysis. More detailed documentation of the applied algorithms is provided along with the source code https://github.com/robna/ImmobileParticles_MatchAndAnalyse

Initial particle detection		<ul style="list-style-type: none"> particles get separated from background by thresholding with hysteresis [43] <ul style="list-style-type: none"> – a lower threshold is calculated using Otsu's method [44], which selects full particle areas – areas are accepted as particles if > 10% of their pixels also exceed a higher threshold fixed at 75% maximum brightness
Finding corresponding particles		<ul style="list-style-type: none"> image registration: pre- and post-images get aligned <ul style="list-style-type: none"> – particles found in pre- image are matched to equivalent particles in post-image if present
Obtaining particle properties		<ul style="list-style-type: none"> matched particles get measured on pre- / post-images measurements are used to compute change rates of properties

Using a positive control for calibration of particle detection The task of the automated image analysis is to discriminate particles from background and match corresponding particles in pre- and post-treatment images. In case a treatment would have destroyed particles, marks in the resin layer are expected to remain visible in the post-treatment image (e.g. a depression where the particle was sitting) and could potentially be falsely classified as a particle. Hence, the detection method has to be capable of distinguishing depressions from actual particles as well. For this purpose, as a positive control, we used one additional wafer with PA6 particles. This wafer was submerged in hydrochloric acid (37%) for 20 min at room temperature (which was shown to completely dissolve PA6, [14]). Pre- and post-imaging, as well as any rinsing steps were conducted as described above. The images that were obtained of this wafer are shown below (Fig. 3). They also serve as a general example of the type of image material that the quantitative part of this study is based on.

The destruction of the particles was confirmed by Raman microscopy (Renishaw, inVia Qontor, laser: 532 nm). Twenty randomly selected depressions in the epoxy layer were analysed, where no distinct PA6 spectrum was present in 17 out of 20 cases (85.0%). In places where PA6 attributed bands could still be detected, a visual microscopic inspection revealed that particle structures were no longer clearly recognisable, indicating that only residues of the PA material were left. This shows that the HCl treated PA6 wafer can be regarded as a

suitable positive control where $\geq 85\%$ of particles were effectively removed and can be used for calibration of the particle detection algorithm. Translated to a non-embedded particle system (e.g. suspensions) where particles would be exposed to the digestant from all sides, this is likely to be a complete particle loss.

The calibration of the particle detection algorithm was conducted on several parameters, most notably the upper brightness threshold, the tolerated displacement and particle size limits. For various combinations of values of these parameters, the resulting particle numbers detected in the pre- and post-treatment images of the positive control wafer were compared with the goal of identifying the parameter set that produced the lowest false positive and false negative errors. Because particles were intentionally destroyed on this wafer, false positives are equivalent to features being recognised on the post-treatment image, while false negatives correspond to particles remaining undetected on the pre-treatment image, despite being obviously present to a human observer. This optimised parameter set was then used for the particle detection in all other images and can be viewed in the source code.

The calibrated image analysis resulted in a particle count reduction of 85.2% ($n_{\text{matched}}/n_{\text{pre}} = 30/203$), which corresponds to the visually and Raman spectroscopically determined particle loss of 85%. In the 30 remaining particles the average area was reduced by 86.3% ($A_{\text{post, matched}}/A_{\text{pre, matched}} = 320/2332 \mu\text{m}^2$, compare Fig. 6). For this fraction it remains unclear whether the particles had

been destroyed incompletely (thus, identified correctly), or misidentified as false positives, despite having been removed. This can occur due to the misidentification of depressions with bright embedded air bubbles or optical artefacts (e.g. bright halos appearing around depressions, see also Fig. 3 bottom images), which could not be avoided. This sets a measurement uncertainty, and if any of the tested treatments would have caused an equivalent reduction in particles, it should ultimately be interpreted as a complete destruction.

Data analysis

As the number of particles per imaged wafer was not constant, measured values of counts and particle area are reported as relative changes. In counts (n) they are calculated from the number of particles in a pre-treatment image which could be matched to a particle present in the corresponding post-treatment image in relation to the total pre-treatment particle count. A relative particle loss $L_{rel.}$ is calculated according to Eq. 1, ranging from 0.0 (all particles were matched) to 1.0 (all lost). Particle areas were aggregated as the mean area per matched particle \bar{a} in both, pre- and post-treatment images, whereof relative changes $C_{rel.}$ were calculated (Eq. 2).

$$L_{rel.}(n) = 1 - \frac{n_m}{n_{pre}} \quad (1)$$

$$C_{rel.}(\bar{a}) = \frac{\bar{a}_{post}}{\bar{a}_{pre}} - 1 \quad (2)$$

Where

n_{pre} = number of particles in pre-treatment images.

n_m = number of particles that could be matched between pre- and post-treatment images. Indices for a alike.

Statistics Influences of non-treatment factors, such as varying contrast and image quality as well as available particle number on a wafer, appeared to have confounding effects on the successful particle recognition and matching. These factors were formalised as n_{pre} being the total particle count that could be identified on a particular wafer before treatment exposure on the one hand, and a range of image histogram obtained variables (Table 5), on the other.

Generalised linear model (GLM) residual analyses were used to estimate and remove these impact of the confounding factors. For an application-oriented introduction and references for further reading on GLMs, we recommend the website of the statistical package statsmodels [45], which was used here for the model calculations. The models followed the form of Eq. 3, with X being an $i \times j$ matrix of the linearly combined independent explanatory variables (predictor terms), y being the dependent response variable and $g(\cdot)$ some function of the conditional expectation of the response, that links it to the linear term of p predictors multiplied with individual coefficients β_j .

$$g(E(y = y_i | X = x_i)) = \sum_{j=0}^p \beta_j \cdot x_{ij} \quad (3)$$

For particle count losses, the binomial distributions for particles matched (successes) and lost (failure) were used as the dependent variable. The model was fitted to the predictor terms using a logistic link function (as given in

Table 5 Image quality related attributes tested as explanatory confounding factors in the statistical modelling applied to the quantitative particle data. Lo = lower threshold as calculated by the particle hysteresis detection algorithm. ^a chosen as suitable for modelling of influences on particle count loss, ^b chosen as suitable for modelling of influences on particle area change, ^c used for calculation of the background distortion index (BDI)

Name	Description	Mathematical Expression
pre_histBGpeak	pre-treatment image background brightness	grey value at the local histogram maximum between but not including 0 and Lo
pre_histFGpeak	pre-treatment image foreground brightness	grey value at the local histogram maximum between but not including Lo and 255
post_histBGpeak	post-treatment image background brightness	grey value at the local histogram maximum between but not including 0 and Lo
post_histFGpeak	post-treatment image foreground brightness	grey value at the local histogram maximum between but not including Lo and 255
pre_histDelta ^a	contrast spreading between the image background and foreground prior to treatment	$\text{pre_histFGpeak} - \text{pre_histBGpeak}$
histBGpeakSum ^c	combined background brightnesses	$\text{pre_histBGpeak} + \text{post_histBGpeak}$
histBGpeakDist ^{b, c}	mismatch between pre- and post-treatment background brightness	$ \text{pre_histBGpeak} - \text{post_histBGpeak} $

Eq. 4, with π_i being the probability of a single success, which is equivalent to the predicted response \hat{y}). For particle areas the absolute mean of area changes of each wafer was modelled using an identity link of the mean μ (Eq. 5) assuming a *Gamma* distribution.

$$g(\pi_i) = \ln \left(\frac{\pi_i}{1-\pi_i} \right) = \ln \left(\frac{\hat{y}_{i,n_{matched}}}{\hat{y}_{i,n_{lost}}} \right) \quad (4)$$

$$g(\mu) = \mu \quad (5)$$

The model was optimised by systematically varying the type and number of employed predictors, whereby the final set was chosen according to the significance of the obtained coefficients, the models deviance and general logic explainability of the ensemble. For both models (count loss and area change) n_{pre} was chosen as one predictor. A second predictor was chosen from the set of image quality related attributes and is indicated with asterisks in Table 5.

The resulting model setups are shown in pseudo-formula notation in Eq. 6 and Eq. 7 for the count loss and area change GLM respectively.

$$particle_counts[successes, failures] \sim \beta_0 + \beta_1 n_{pre} + \beta_2 pre_histDelta \quad (6)$$

$$area_change \sim \beta_0 + \beta_1 n_{pre} + \beta_2 histBGpeakDist \quad (7)$$

The predicted response was then taken as the portion of particle loss caused by the confounders, whereas the responses standard residuals were regarded as the remaining unexplained, hence treatment-attributed portion of the effect. Only where the residuals exceeded the 95% prediction interval of the water fitted response, effects were interpreted as significant.

Besides for the GLM models the image quality predictors (Table 5) were also used to calculate a generic index (background distortion index, BDI, see Eq. 8) providing a rough estimation of contrast problems due to the image background brightness level. The index number is higher for image pairs of worse quality. It was used for illustration purposes and to determine a limit of which images are not of acceptable quality and need to be excluded from analysis. The two coefficients α and γ were empirically found by optimising an ordinary least squares regression of relative particle losses against BDI. The calculated BDIs were normalised to range from 0 to 100, in order to be independent of the average image brightness. A BDI of 0 corresponds to the best and 100 to the worst image quality present.

$$BDI = \alpha \text{ histBGpeakSum} + \gamma \text{ histBGpeakDist} \quad (8)$$

with $\alpha = 2$, and $\gamma = 9$.

Using negative controls for method uncertainty estimations As a negative control, one wafer per polymer type was exposed to ultra-purified water (see Table 2). The GLMs were trained using an iteratively reweighted least squares algorithm [46] on the set of the negative control samples (see SI (S2) for details).

Results and discussion

Qualitative analysis

Commodity polymers

Overall, none of the post-treatment polymer spectra, both in FTIR and Raman, showed substantial spectral band changes that would hinder recognition (Fig. 4, Commodity polymers). However, minor alterations were detected in several cases, which are further detailed below.

Using Raman, increased fluorescence or baseline shifting (category 1 changes) were the most frequently seen effects, but did not hinder a successful recognition of the MP's polymer type. Only for PVC in the H_2O_2 Fe uncooled treatment clear degradation effects on the polymer basis became visible in multiple measured replicate spectra. Two peaks around 1124 and 1511 cm^{-1} ($C=C$ double bonds) strongly increased, which are a direct result of the dehydrochlorination reaction due to thermooxidative processes [47]. It is noteworthy that these degradation processes appear to affect individual PVC particles differently, as we see from the varying spectral characteristics between the replicate measurements (see also deposited spectroscopic data at <https://doi.org/10.5281/zenodo.4568683> [34]) and also from varying degrees of visual yellowing from white over beige to yellowish brown across particles.

In 10 out of the 125 Raman measurements multiple new peaks appeared which could not be attributed to specific functional group frequencies and were therefore not regarded as a polymer related change (these cases are indicated by * in Fig. 4, compare annotated deposited spectra [34]). These peaks were treatment and polymer unspecific and most frequently appeared in the water control. This led to the suspicion that the water, used to rinse after the treatment, introduced the impurities. Switching to ultra-purified water for the remaining tests (i.e. H_2O_2 LT, Pentane, SPT) completely prevented these unknown peaks. They do not carry exploitable information for the question of polymer recognisability and their emphasis in Fig. 4 merely serves the purpose of clarity when comparing the here presented results to the original spectra provided in the deposited spectra [34].

In FTIR, the polymer basis was always clearly identifiable. We detected, however, minor polymer degradation processes in the H_2O_2 LT treatment. This concerned ABS, PC, PMMA, PP, PVC, TPU where new bands could be assigned to carboxylic acids which may have

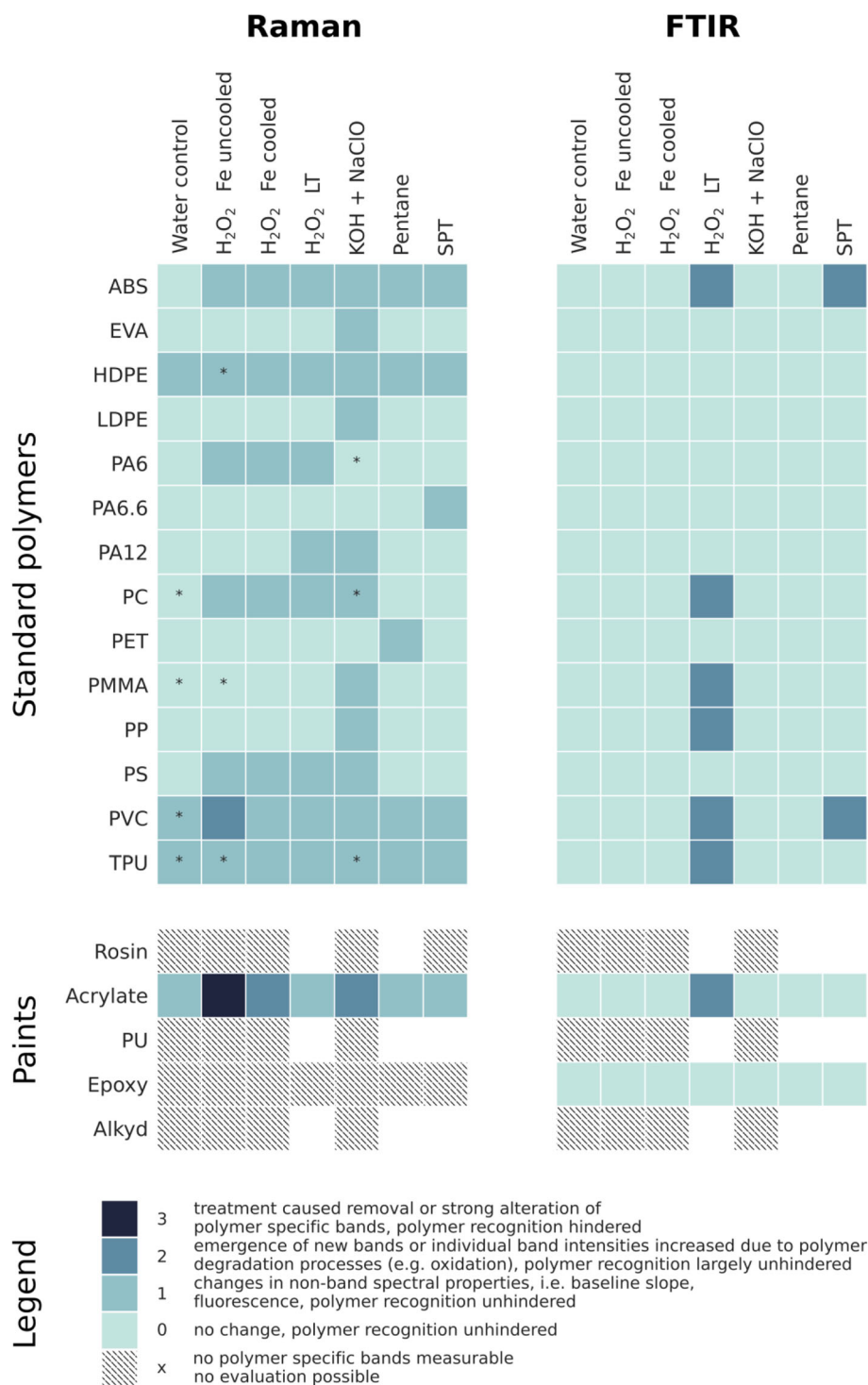


Fig. 4 Spectral changes expressed as categories as they were assigned by manually comparing the post-treatment spectra to the pre-treatment references. Asterisks (*) indicate spectra with newly evolved bands which, however, could be traced back to inorganic impurities originating from the rising water (not used in category assignment). White tiles indicate data not available (measurements were not taken due to expected unexploitable spectra, as other measurements of the same polymers indicated)

resulted from oxidising polymer chain ends. In the SPT treatment, similar oxidations were observed for ABS and PVC. The corresponding Raman spectra, however, did not systematically indicate these changes. This is plausible as FTIR is sensitive to polar organic groups, such as $C=O$ and its variations (e.g. esters, anhydrides, amides, imides), while Raman is less sensitive to these.

It appears that for FTIR category 2 changes occur rather treatment-specific, whereas for Raman spectra no treatment-specific impacts were seen. Instead, several cases of category 1 effects appeared in a rather polymer-specific manner. Although category 1 effects were also found in the water control of HDPE and TPU, it is noticeably the actual treatments that got assigned to this category.

As Fig. 5 shows, the HQI of the treated samples lie in the range of the untreated reference for most tested polymer types. For some treatments, the HQI range of the replicates varied more than for others. In the case of LDPE, the HQI distribution reflects the assignment of the categories (compare Fig. 4). That is, the KOH + NaClO treatment introduced category 1 changes, while no significant changes occurred in the other treatments. Only for KOH + NaClO, the HQI drops to around 90–59 for the different replicate

spectra. Similarly, the correct material type was found amongst the first ten hits in the library search, except two single replicates of a polymer-treatment-combination. One pentane-treated HDPE was identified as aliphatic fatty acid or alcohol. This is, from our experience, a frequently occurring problem in Raman spectroscopy. This and the fact that it only happened for one in three replicates should not lead to classifying the pentane treatment as harmful for this polymer type. The second not correctly identified spectrum resulted from a KOH + NaClO-treated PET replicate. Here, the occurrence of the inorganic contaminant calcium carbonate led to extra bands that prevented a semi-automated polymer identification. Overall, this confirms the assumption that none of the treatments induced changes that prevented the identification by a manually supervised spectral library search, as it is common in microplastics research. The result of a HQI based polymer attribution depends, however, on the available references, the applied algorithm and search parameters. It is not generalisable between studies and laboratories and therefore not used as a systematic evaluation criterion here.

In summary, our qualitative results indicate that, regarding the spectroscopic recognisability of MP

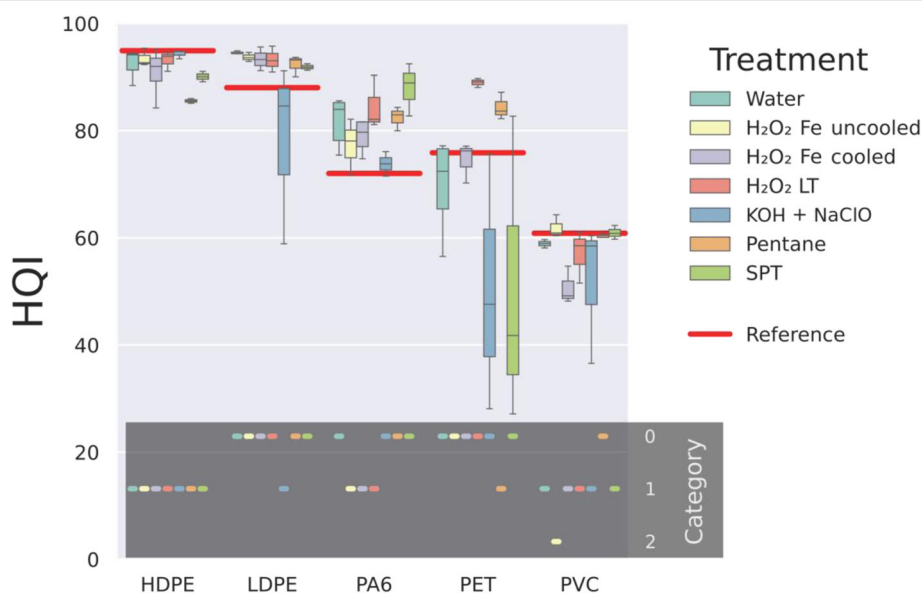


Fig. 5 Raman Hit quality indices (HQI) were measured on a subset of polymers for all treatments against a commercial library (ST Japan). Red lines (Reference) indicate which HQI level was reached using a spectrum of the untreated material of the respective polymer. Boxes show median HQI and .25 / .75 percentiles of a set of replicate spectra, $n \geq 3$. The grey box at the bottom provides the assigned qualitative categories for comparison. Note that categories were assigned in a manual spectral evaluation process and deliberately not based on the HQI values. Apparent discrepancies are discussed in the text. Both, manual categorisation and achieved HQI values, are resulting in the same predicate regarding polymer recognisability: the tested treatments do not alter spectra in a way that a successful polymer identification would be hindered

particles of any of the tested commodity polymers, all of the tested treatments are safe to apply, when the chosen analysis technique is either FTIR or Raman spectroscopy. However, effects on the treated polymers spectra, that were less critical to polymer recognition (i.e. category 1, Table 3), occurred frequently. Raman baseline shifts can be caused by heating of the sample during measurement [48]. Fluorescence mainly originates from sample characteristics, but background conditions such as ambient lighting, can play a role as well [49]. Both effects are too unspecific to be assigned to a polymer degradation process. Changes in the ATR-FTIR baseline can occur due to multiple changes in the optical path, e.g. the contact between the sample and the ATR crystal. They reflect physical rather than chemical changes, and again, are not fit to indicate a change in the polymer composition.

Paint resins

Out of the five paints, in all but one (acrylate) the polymer resin was not identifiable, already in the pre-treatment Raman spectra. In the KOH + NaClO as well as in the H₂O₂ Fe cooled treatment acrylate showed effects of degradation, however, was still recognisable. After the uncooled H₂O₂ Fe treatment, however, the polymer related bands were not found any longer, making an identification impossible. All other four paint spectra were substantially masked by fluorescence in both pre- and post-treatment spectra. In some cases, pigments (inorganic bands) dominated the spectra. One black (PU) and one grey paint (alkyd) showed an additional band which is indicative for black carbon (1343 cm⁻¹ and 1581 cm⁻¹, [47]). But as black carbon can stem from various sources in environmental samples, without any signal of the polymer bases the Raman spectra of these paint resins are unspecific and an identification by an automated detection procedure is not possible. As a result, no conclusions can be drawn concerning effects of the tested treatments on the polymer bases and associated processes of polymer degradation based on Raman spectroscopy.

The polymeric binders were clearly detectable for acrylate and epoxy based paints using FTIR spectroscopy. In these paints none of the treatments lead to a change in spectral quality, except the H₂O₂ LT treatment, which introduced carboxylic acid salt signatures around 1600, 1350 and 789 cm⁻¹ in acrylic paint, indicating polymer oxidation processes. While for PU based paint no exploitable spectral properties could be found in neither pre- nor post-treatment spectra, the paints based on rosin and alkyd exhibited some weaker bands that could be attributed to the organic binder matrix by an experienced spectroscopist,

however not with sufficient confidence. Hence, we note that only the epoxy and the acrylic paint can be regarded as reliably identifiable by their polymer FTIR bands and are thus useful for evaluating the treatments effects on polymer recognisability. Chemical treatment-caused spectral changes i.e. bands weakening or disappearing were found in acrylic paint for H₂O₂ (Fe + LT) and SPT treatments. This did, however, not hinder the recognition of the polymeric binder as only inorganic components were affected indicating mineral depletion (CaCO₃). Thus, no restricting categories were assigned based on this observation (Fig. 4).

Comparing Raman and FTIR spectra of paints, overall masking was weaker in the FTIR spectra. Where peak changes were present, they were dominantly caused by pigments or other fillers, for both techniques. Only for acrylic paint the strong thermo-oxidative regime of high temperature Fenton's catalysed H₂O₂ treatment made an unambiguous spectral recognition impossible in Raman, however not in FTIR.

In paints based on rosin, polyurethane and alkyd the detection of binder matrix bands was not possible already on the untreated material (at least not to a degree of certainty that would allow the identification if the material was unknown). Thus, degradative effects of the treatments cannot be studied with the here applied techniques. Our conclusions are limited to the observation that in general a reliable detection of paint flakes of these resins using spectroscopic identification is not guaranteed. In contrast to commodity plastics, paint resins are typically composed of high amounts of non-polymeric constituents and only a smaller portion of the polymer itself. Accordingly, it is questionable whether paint resins can be exhaustively and reliably identified in environmental systems using spectroscopic methods [20, 50]. The chemical bonds of many inorganic and organic pigments and other paint constituents are strong Raman scatterers, which renders them well detectable in Raman spectra (also better than with FTIR). On the downside they frequently mask the weaker bands of the polymeric binder due to their strong intensities or additional fluorescence. Large reference libraries containing spectra of large varieties of paint composites preferably from different manufacturers might be able to detect paint flake MP based on their (pigment dominated) fingerprint. This approach has also been taken by other studies [13, 51]. Most pigments are, however, not solely applied in synthetic polymers but in a large diversity of technical applications, which is why an indirect identification of MP via those pigments cannot be done in a systematic way. Furthermore, due to the large variety in different paint compositions, an automatic detection is limited unless the particular paint product is available in the spectral library.

Quantitative analysis

Particle property comparisons

As for the qualitative data, a high level overview on the quantitative data can be gained from the heat maps that summarise the relative changes that we could attribute to the treatments (Fig. 6). Noticeable are elevated values present in various polymers exposed to the H_2O_2 treatment. Further, for ABS, PC and epoxy based paint there are higher values found across treatments.

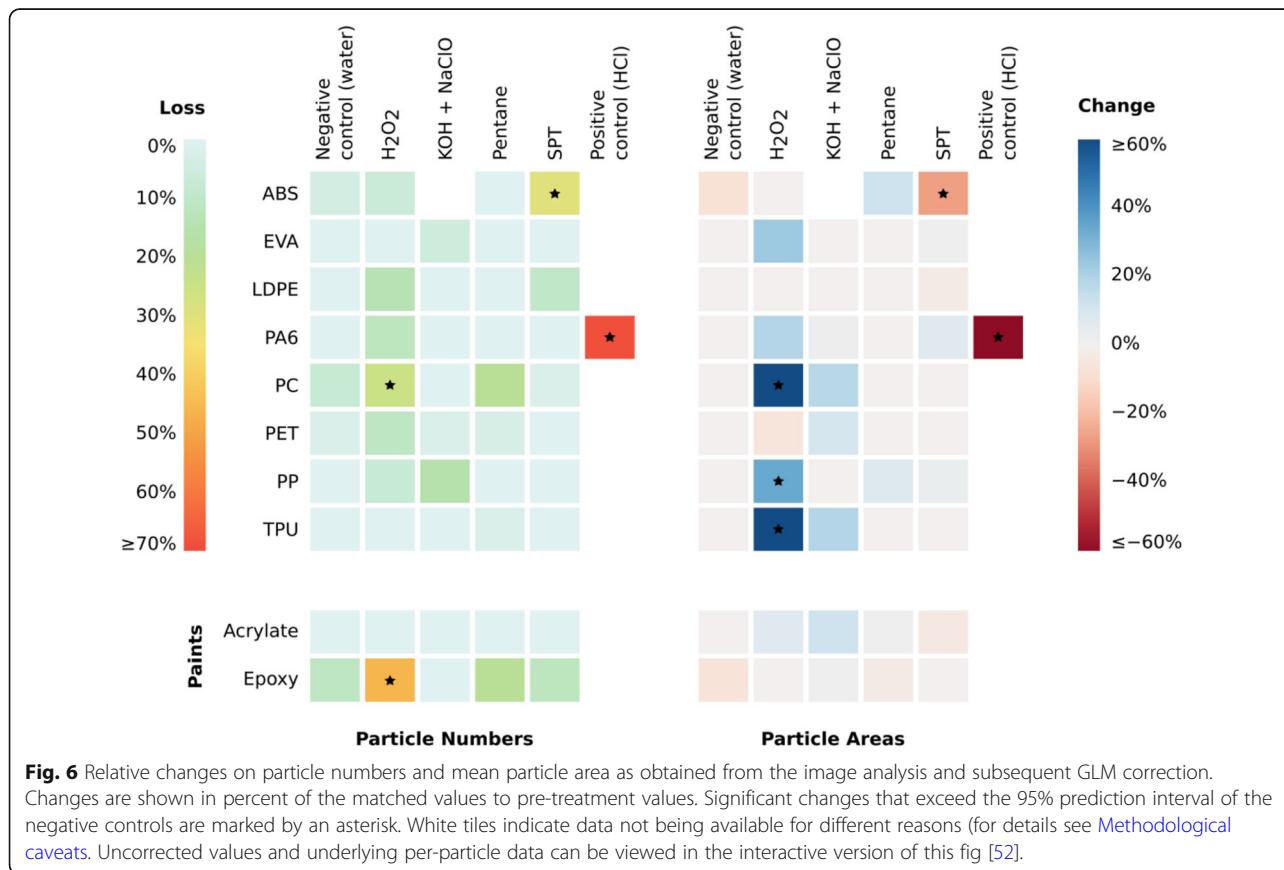
To enable a deeper insight into the quantitative dataset, we provide an interactive version of the heat map figures (Fig. 6), augmented with plots of individual particle data showing detailed and aggregated differences between pre- and post-treatment images. It may also be used to understand the necessity and effect of the GLM corrections that were applied to the data. The interactive figure may be downloaded from: <https://doi.org/10.5281/zenodo.4568524> [52].

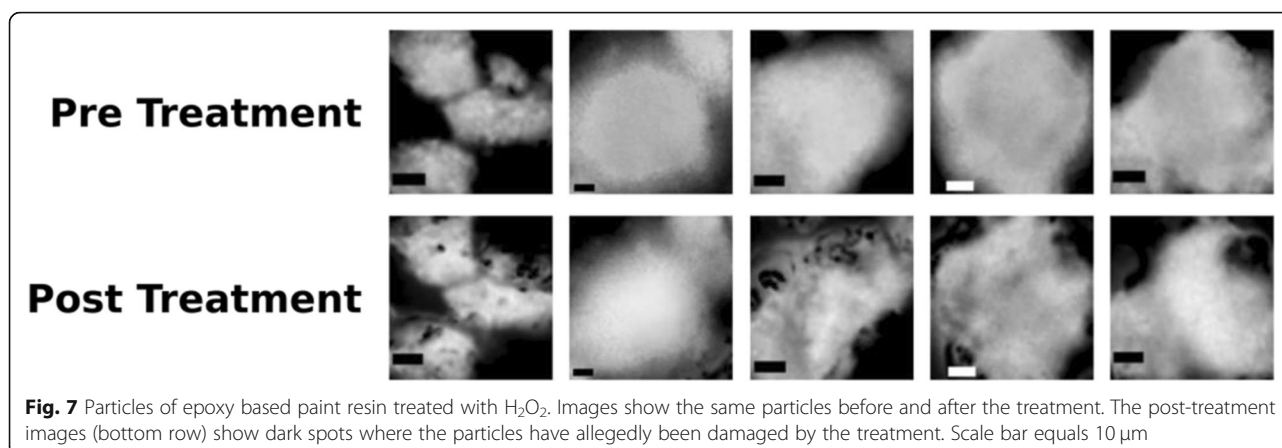
Particle counts From the GLM corrected data, it can be seen that the majority of polymer treatment combinations did not show any loss significantly different from the negative control. Exceptions are the SPT treated ABS (30%) and the H_2O_2 treatments of epoxy based paint and PC (46% and 25%, respectively). For these three polymers also the

corresponding water treatments show particle losses higher than any of the other polymers. This indicates that for images of these polymers not all of the confounding effects could be removed by the GLM correction, and the actual treatment caused changes must be lower.

For the H_2O_2 treated epoxy paint particles we conclude that the relative loss in the GLM corrected data is indeed indicative of an actual treatment caused effect. Influences of confounding factors were comparably low for this image pair ($n_{pre} = 212$, $BDI = 0$). The modal value of particle brightness is reduced in the post-treatment image ($pre_histFGpeak = 183$ and $post_histFGpeak = 103$ out of maximum of 255, respectively, see Table 5 for explanations), indicating a possible material erosion, which could not be explained by other factors. This is further substantiated by looking at individual particles in a pre-post-comparison, where dark indentations or holes become visible, in places where the particle surface or boundary were priorly intact (Fig. 7).

It is known that certain polyepoxides are susceptible towards peroxides, in fact, this is utilised in certain technical applications. One study used 24% and 50% H_2O_2 to superficially degrade epoxy resins and expose embedded fibres in a fibre reinforced polymer (FRP) [53]. For the recycling of carbon fibres from FRPs, acetified H_2O_2 (30%) was





deemed effective for an epoxide matrix decomposition in an overnight treatment [54]. When epoxy resin particles are targeted within environmental MP studies and peroxide digestion protocols are applied, we recommend for future studies to note that numbers are likely underrepresenting the actual environmental load for these polymers. In our data the corrected particle loss exceeded that of the epoxy water digestion by 35 percentage points. Hence, it can be assumed, that a reported concentration of epoxy MP particles in a certain environment are only covering approximately 65% of the total load present, at least for particles in the here studied size range.

The effect of H_2O_2 could also be seen on the epoxy layer that we used to immobilise the particle on the Si wafers. Increased brightness and haziness of the image background was apparent especially around the wafer edges, which made more encroachments by manual image postprocessing necessary in those wafers. Small defects in the layer were promoted to brighter visual appearances after the treatment that could lead to false positive detections, while increased brightness in the near field surrounding of particles, is likely a contributor to the observed particle area growth that was observed in several H_2O_2 treated polymers. These effects on the layer show that with the epoxy resin used here, we have not yet found the optimal immobilisation adhesive for the purpose of the study. We argue though, that the effects do not constitute a failure of the immobilisation technique, as we know from the positive control wafer (PA6 treated with HCl) the detailed visual characteristics of spots where particles got removed from the layer. Such appearances were not what we could typically observe in the images of H_2O_2 treated wafers, instead, the image objects at places where particles were expected generally resembled what particles looked like in the other treatments (including the negative control water treatment). This is yet not sufficient evidence to fully exclude that a loosening of particles may have occurred in some places due to the layer being affected, but it shows the this was not predominant process. Hence we conclude: the spin-

coated epoxy layer did resist our H_2O_2 treatment at least to a degree that particles could be held in place and measured after the treatment. It could be further improved by finding an adhesive composition that does not show any visual nor integrity-related impacts from any of the tested treatments. Experiences and advice from our adhesive layer development phase are detailed in the SI (S3).

The wafer of H_2O_2 treated PC suffered the problem of having a low total particle number ($n_{pre} = 26$), which could not be entirely alleviated by the applied GLM correction. The particle brightness was not reduced on this wafer after the treatment (pre_ and post_histFGpeak were at 88 and 89, respectively), suggesting that there was no treatment caused effect acting on all particles collectively. Instead the loss was driven by only six particles that could not be matched between the images. The low n_{pre} is thus regarded here as the main reason for the resulting significant loss.

The loss of particles from the SPT treated ABS wafer should only with certain reservations be seen as an indicator of particle degradation, as the image quality was on the brink of our exclusion level ($\text{BDI} = 26$). We interpret the observed losses as partly treatment caused and discuss this interpretation below (Comparison of qualitative and quantitative results).

Most prominent, but also expected, is the loss of nearly all particles in the positive control wafer (HCl on PA6), where 69% of pre-treatment particles could no longer be confirmed to be present post treatment (85%, without GLM correction, see also Using a positive control for calibration of particle detection).

Particle areas In contrast to particle counts, changes of particle area were recorded to differ in negative (area decrease) as well as positive (area increase) direction. The largest decrease of particle area can be seen in the positive control, however, also the SPT treated ABS was recorded with a significant area reduction of 30%. But as noted above, one should take this result with caution,

due to the low image quality of this wafer. Several polymers treated with H_2O_2 revealed significant area increases post treatment (PP, TPU and PC with a 34%, 60% and 220% average increase, respectively). The extreme increase in particle area of PC was mostly caused by two outliers where in the pre-treatment image the particle was only partly detected by the thresholding algorithm. An increase in area or particle volume would not hinder a MP detection, however, it may lead to a distorted representation of particle sizes.

For the H_2O_2 treated epoxy paint particles, where we described a significant particle loss above, we do not see a change in area for the remaining matched particles. The formation of dark holes in particles (Fig. 7) is not represented in the post-treatment area measurements, because particles are identified as closed shapes by the detection algorithm.

Methodological caveats

The here presented technique for quantitative MP treatment evaluation was limited in two ways. Limitations were caused either by effects of a specific treatment on the adhering epoxy layer, or, by polymer specific characteristics which impeded a contrast rich DIC imaging.

The KOH + NaClO treatment disrupted the adhesion between the spin coated layer and the underlying Si wafer, which lead to a partial or complete detachment of the epoxy film and wrinkling artefacts on the images in several cases. The film itself did not seem to be degraded or otherwise affected as microscopic imaging could confirm that the epoxy matrix and attached MP particles were visually intact. However, the correct placement for a post-treatment imaging was disturbed and the layers were partially outside of the microscope's focal plane, which resulted in darker areas that could no longer be recognised by the particle detection. This affected especially the KOH + NaClO treated wafers of PP and PET, where such areas needed be mutually excluded from the pre- and post-treatment images in the manual image postprocessing. The H_2O_2 treatment had a different effect on the epoxy layer, however without affecting the image quality to an extent where the image analysis would be impeded. The wafers treated with H_2O_2 were showing varying degrees of obliqueness in the otherwise clear epoxy layer, indicating a surface affect or softening of the layer. The resulting implications are discussed in the above section.

For PVC, PMMA, PS and, to a lesser degree, ABS the chosen microscopy mode (reflected DIC) was not able to generate images that have a good particle to background contrast. The image postprocessing did increase the particle brightness for the particle detection algorithm but at the cost of a proportionally gained brightness of the image background. For reasons unbeknown to us, the

surface topography of MP particles of these polymers did not create an optical path length difference that would allow for contrast rich DIC images. The size range of the particles of these polymers was not different than for the other polymers and further investigations beyond the scope of the study would be necessary to clarify whether this is indeed due to polymer specific optical characteristics or rather special interactions between the particles and the uncured epoxy layer at the time of application. Unless a solution is found to create particles and immobilisations of these four polymers that yield a sufficient contrast, the more suitable approach would be applying a different microscopic technique. Possible candidates are discussed in the SI (S3).

With the current state of the experimental approach, the polymers of PVC, PS and PMMA, could not be included in the analysis, due to the above-mentioned reasons. PMMA and PVC were excluded due to low image qualities. Of the ABS wafers only the KOH + NaClO treated sample had image qualities that resulted in a BDI exceeding the set cut-off of 27. For PS, however, the BDI was not able to ascertain that the image quality was unsuitable for an analysis, because the image defects in PS were slightly different than in PVC and PMMA. While the latter showed a general and evenly low contrast between particles and background, PS had mostly a stronger contrast but included many optical artefacts (i.e. bright ring-like halos around particles). It was attempted in image postprocessing to remove the artefacts manually, however, the PS images could not be improved sufficiently. Images of PVC and PS can be viewed in the deposited imaging dataset at <https://doi.org/10.5281/zenodo.4568488> [55] as an example of the contrast problems.

The above discussed caveats currently pose certain limitations in terms of applicability, explanatory power and required work effort. The true value, however, is present here as the possibility of the immobilisation approach to study effects on individual particles simultaneously on large particle numbers in the smaller MP size ranges. How this compares to other concepts is discussed below in the section [Comparison of experimental concepts](#). Additionally, in the SI we describe more detailed the lessons learned and attempts to further methodological improvements for interested readers (S3).

Comparison of qualitative and quantitative results

While the quantitative particle data provides insights in the particle-based alterations of a treatment, it does not convey whether these can be recorded by the chosen analysis technique (here Raman and FTIR spectroscopy). As an example, particles might still be present after a treatment, but changes on the surface of the particles or the polymer matrix might render them undetectable.

The other way round - a polymer type is recognised post treatment but the quantitative measurements reveal particle losses or area changes - is also a possible scenario. In fact, the epoxy based paint resin in our data is an example, where we observed a significant particle loss after a 24 h H_2O_2 exposure, while FTIR recorded no changes to the polymer spectrum even after a prolonged 2 weeks' exposure or the uncooled Fenton's with its $80 + ^\circ\text{C}$ temperatures. The two-tiered approach, providing qualitative and quantitative data on the same polymer treatment model systems, therefore allows for a higher certainty on the applicability of the tested treatments. For a comprehensive evaluation both aspects are of importance.

A related study also reported qualitative (spectroscopic) and quantitative (recovery of spiked particles) data [11]. They noted a qualitative change on H_2O_2 treated PVC (see also below section for further details: Comparison of our results to current literature), however could not confirm that the described polymer degradation would manifest in the quantitative measurements.

In our data, SPT treated ABS that was indicating negative changes in particle numbers in the quantitative result, also showed alterations in the spectra of FTIR (assigned category 2, emergence of new bands or band intensities altered), and Raman (category 1, baseline drift). The treatment with SPT resembles a density separation where HCl is used to acidify the solution to pH 3, in order to prevent sodium poly tungstate precipitation [31]. We know that ABS is attacked by acidic digestions [1], however, this was only shown for highly concentrated and strongly oxidative acids (HNO_3 69% and HClO_4 70%), neither of which applies to the here deployed solution. As it was demonstrated there, the acidic treatment lead to a bloating and bubbling dissolution of the macroplastic piece that was tested [1]. The present results indicate an area reduction of those particles that were found again after the treatment. A testable conjecture beyond the scope of this study, is that a count and area decrease was detectable – despite working under a much weaker acidic environment – because of the small size range of particles that were used here, and which potentially are more easily damaged by acids.

Comparison of our results to current literature

To our knowledge, polymer chemical resistance tests in qualitative and quantitative manner have not yet been performed on such small MP particles. Partly related studies reported recovery rates of $>90\%$ of spiked particles using fluorescence-labelled microspheres $\leq 30\text{ }\mu\text{m}$ as representatives of small MP for a novel magnetic separation [12] and in a density separation and digestions [10]. Working with aliquoted pipetting of bulk particle suspensions, they noted that

direct comparisons of the same particles' pre- and post-treatment counts was infeasible in this size range [12]. Generally, our overall finding, that, with respect to spectroscopic recognisability, no considerable changes to the polymeric bands were caused by the tested treatments on $\text{MP} < 70\text{ }\mu\text{m}$, is in agreement with other studies which used larger MP particles. One study tested the same $\text{KOH} + \text{NaClO}$ protocol on a similar set of 12 commodity polymers ($\geq 5\text{ mm}$) and performed Raman spectroscopy on pre- and post-treatment particles, finding no relevant changes on the polymer matrix [1]. Dehaut et al. [5] applied a KOH protocol without an additional oxidiser, also reporting no effect on Raman spectra even at 60°C in all 11 polymers that were comparable between their and our study. Similarly, Hurley et al. [25] found no significant spectral changes applying a Fenton's protocol (cooled, $< 40^\circ\text{C}$) to a set of 8 different commodity polymers ($\sim 3\text{ mm}$) using FTIR.

In our Raman measurements, the only polymer degradative effect was observed in PVC, where the formation of $\text{C}=\text{C}$ double bonds (caused by dehydrochlorination) occurred only in the uncooled H_2O_2 Fe treatment ($> 80^\circ\text{C}$, 10 min) as a direct consequence of thermo-oxidative processes on the polymer matrix (as we also observed in an early study [47]). Likewise, Raman spectra measured by Karami et al. [11] on PVC particles treated with 50°C H_2O_2 were described as being diminished in the $\text{C}-\text{Cl}$ stretching band, which would be indicative of the same dehydrochlorination process that we observed. But, as mentioned above, PVC exposed to 60°C in a KOH based treatment (10%, 24 h) exhibited no effect on Raman spectra [5], albeit the presence of a hydrolytic and thermo-oxidative pressure. The difference lies apparently in the stronger oxidising potential of the H_2O_2 , that induces detectable – but non-critical – polymer degradation of PVC. It should be noted though, that the occurrence of PVC thermo-oxidative degradation depends on the specific PVC material and its added stabilisers. It is plausible that for other PVC compositions this effect may be induced alone by temperature rises above 60°C .

In general, negative impacts of elevated temperatures during treatments have also been demonstrated by various studies. For instance, increased mass loss for PA in H_2O_2 (among other treatments), was reported for temperatures between 60 and 70°C [14] and for $> 70^\circ\text{C}$ [25]. In our qualitative analysis PA did not show signs of degradation, however, we cannot infer whether particle losses or area changes may have resulted from these treatments, as no treatments involving elevated temperatures were part of our quantitative analysis. Yet, the non-catalysed H_2O_2 treatment (room temperature) resulted in no change of PA6 particle numbers or areas.

For the pentane treatment [31] we could now demonstrate polymer resistivity among our test series. The protocol, which involves a weakly acidic digestant (ethanol acidified to pH 3 using acetic acid is added to the sample before pentane), had no impact on the spectra of any of the tested polymers, hence also not on the polyamides, known to be susceptible to acidic degradation. PA6 particles, which we tested quantitatively, suffered no detectable impact by the pentane treatment in particle numbers or areas. Similarly, the acidic SPT was not affecting particle numbers or sizes, except for ABS, where a minor degradative effect could not be excluded, based on our data.

It was reported that PA6.6 melted when applying H_2O_2 at 70 °C and a significant weight and size loss was measured [25]. In our uncooled catalysed H_2O_2 treatment (reaching up to 85 °C for the 10 min treatment duration) PA 6 showed a yellowing effect despite not showing significant quantifiable losses in size or area. Potentially, the temperature exposure in our treatment was not long enough to melt the polymer compared to their exposure time (12 h).

Studies exist that found degradative effects of alkaline protocols on PET [5, 14, 25], however also other factors such as elevated temperatures were involved in some of these cases. Our qualitative results of the protocol using KOH + NaClO do not show signs of degradation of PET in FTIR or Raman spectra; neither do we see a significant particle loss or area change in the quantitative data. The quantitative are, however, of lower confidence, as these samples were affected by the KOH + NaClO induced displacement of the epoxy layer, complicating image analyses.

Comparison of experimental concepts

To our knowledge, working with particles immobilised by adhesives to obtain quantitative measurements has not been performed so far. A related approach was developed recently for measuring PS nanoplastic spheres, where etched cavities in Si wafers were serving as a nanofabricated grid [56]. Particles placed in suspension on the cavity array were assembling by capillary forces and thus temporarily arrested for subsequent material and size determination using Raman spectroscopy. Alternative approaches to microscopy have been applied to determine size changes, such as laser sizing [57]. However, when measuring in wet dispersion problems can arise for polymers with a lower density than water as a sufficient particle dispersion can be challenging to achieve. Absolute particle counts cannot be determined using this technology and problems can arise if post-treatment particle numbers fall below the measurement limit of the specific laser sizer [57]. Also Coulter counters or flow cytometry, might be suitable techniques for

these kind of measurements. Usually applied for counting plankton or cells, they allow simultaneous count and size measurements. A disadvantage, however, is the necessity for a filtration step to purify the particles for a post-treatment measurement. Finally, direct microscopic imaging of filtered bulk particle suspensions before and after a treatment could be a viable approach as well. However, like all methods using mobile particles entails the problem, that count data is difficult to obtain for small-sized MP. Particles can get lost in transfer steps and effects like breaking apart, aggregation, handling loss or real treatment-caused degradation are difficult to disentangle. This has been observed by others as well. Thiele et al. [13] used MP particles < 600 µm (that could still be manually handled) for spiking and recovery tests in a treatment evaluation and reported issues with particle loss in transfer steps that needed to be mathematically accounted for. With an immobile particle approach these problems do not arise.

Conclusion

We identified the need in the scientific community for a method to evaluate the impact of treatment procedures on MP particles that are smaller than what can be easily be handled manually, e.g. using fine-tipped tweezers. Studies which aim at identifying MP in the lower µm sizes rely on the certainty that the investigated MP particles are not destroyed by the chosen sample purification protocol.

In summary, we could show that conducting treatment evaluations with immobilised MP particles in the lower micrometre sizes is possible and has a range of advantages. From a theoretical perspective this could be readily adapted for even smaller MP and nanoplastics. In contrast to mobile particle approaches, particle properties changing due to a treatment can be studied here on individual particle level.

For the first time it was possible to demonstrate for MP as small as 10 µm, that purification methods, which are already routinely used, do not substantially alter the spectroscopic detectability, nor quantitative properties for many of the most common polymer types. Our results substantiate the validity of applications that extract particles in this size range by those methods. It turned out that polymer resins used as binders in synthetic paints are distinct from MP derived from commodity plastics. In chemical treatments they were more easily taking damage and their spectroscopic recognisability was severely limited independent of treatment. A tentative conclusion hereof is that numbers of paint flakes, found in environmental samples, are likely to be underestimated compared to other MP species.

We recommend that future studies take up the approach – and lessons learned – for qualitative and quantitative evaluations on immobilised MP, to yield further certainty of applicability of their respective methodological setups.

Abbreviations

MP: Microplastic(s); BDI: Background distortion index; DIC: Differential interference contrast microscopy; FRP: Fibre reinforced polymer(s); FTIR: Fourier transform infrared spectroscopy; GLM: Generalised linear model(s); HQL: Hit quality index; Lo: Lower threshold; LT: Long term; RT: Room temperature; SI: Supplementary information; SPT: Sodium polytungstate

Supplementary Information

The online version contains supplementary material available at <https://doi.org/10.1186/s43591-021-00012-0>.

Additional file 1.

Acknowledgements

For helpful comments and expertise, we thank Klaus-Jochen Eichhorn, Mikhail Malanin and Lars Bittrich. Support in laboratory work was kindly provided by Elisavet Kanaki, Pia Ullischberger, Anne Rödiger, Piotr Jachimowicz, Julia Muche and Juliana Ivar do Sul.

Authors' contributions

RL, KE, DF and ML developed the idea for this research; RL, KE, and FF contributed the conception and design of the work; RL, KE and FF conducted the acquisition, analysis and interpretation of data; RL and JB created new software used in the work; JB provided code revision; RL, KE and FF have drafted the manuscript; JB, DF and ML substantively revised it. The authors read and approved the final manuscript.

Funding

Funding of this study was received from the project MicroCatch_Balt (German Federal Ministry of Education and Research (BMBF), grant number 03F0788A) and the BONUS project Micropoll (funded jointly by the European Union and the BMBF, grant number 03F0775A). Open Access funding enabled and organized by Projekt DEAL.

Availability of data and materials

- The source code of the image and statistical analysis and visualisation is available as a static archive on Zenodo [35] with the identifier <https://doi.org/10.5281/zenodo.4592319> and as a repository on Github at https://github.com/robna/ImmobilizedParticles_MatchAndAnalyse
- The interactive figure that was used for the exploration and analysis of the quantitative dataset of this study is available on Zenodo [52] with the identifier <https://doi.org/10.5281/zenodo.4568524>
- DIC microscopy data that support the quantitative findings of this study are available on Zenodo [55] with the identifier <https://doi.org/10.5281/zenodo.4568488>. This includes all pre- and post-treatment images after manual processing and downscaling (as used in the analysis). Original raw imaging data is not provided there due to large file size (> 1 TB), but are available upon reasonable request from the authors.
- The Raman and FTIR spectroscopy data that support the qualitative findings of this study are available on Zenodo [34] with the identifier <https://doi.org/10.5281/zenodo.4568683>.

Declaration

Competing interests

The authors declare that they have no competing interests.

Author details

¹Leibniz Institute for Baltic Sea Research Warnemünde, Seestraße 15, 18119 Rostock, Germany. ²Leibniz Institute of Polymer Research Dresden, Hohe Straße 6, 01069 Dresden, Germany. ³University of Gothenburg, Department of Marine Sciences, Kristineberg 566, S-45178 Fiskebäckskil, Sweden.

Received: 15 March 2021 Accepted: 17 June 2021

Published online: 18 July 2021

References

1. Enders K, Lenz R, Beer S, Stedmon CA. Extraction of microplastic from biota: recommended acidic digestion destroys common plastic polymers. *ICES J Mar Sci.* 2017;74(1):326–31. <https://doi.org/10.1093/icesjms/fsw173>.
2. Tagg AS, Harrison JP, Ju-Nam Y, Sapp M, Bradley EL, Sinclair CJ, et al. Fentons reagent for the rapid and efficient isolation of microplastics from wastewater. *Chem Commun.* 2017;53(2):372–5. <https://doi.org/10.1039/c6cc08798a>.
3. Löder MGJ, Imhof HK, Ladehoff M, Löschel LA, Lorenz C, Mintenig S, et al. Enzymatic purification of microplastics in environmental samples. *Environ Sci Technol.* 2017;51(24):14283–92. <https://doi.org/10.1021/acs.est.7b03055>.
4. Kühn S, van Werven B, van Oyen A, Meijboom A, Rebolledo ELB, van Franeker JA. The use of potassium hydroxide (KOH) solution as a suitable approach to isolate plastics ingested by marine organisms. *Mar Pollut Bull.* 2017;115(1–2):86–90. <https://doi.org/10.1016/j.marpolbul.2016.11.034>.
5. Dehaut A, Cassone A-L, Frère L, Hermabessiere L, Himber C, Rinnert E, et al. Microplastics in seafood: benchmark protocol for their extraction and characterization. *Environ Pollut.* 2016;215:223–33. <https://doi.org/10.1016/j.envpol.2016.05.018>.
6. Avio CG, Gorbi S, Regoli F. Experimental development of a new protocol for extraction and characterization of microplastics in fish tissues: first observations in commercial species from Adriatic Sea. *Mar Environ Res.* 2015;111:18–26. <https://doi.org/10.1016/j.marenvres.2015.06.014>.
7. Nuelle M-T, Dekiff JH, Remy D, Fries E. A new analytical approach for monitoring microplastics in marine sediments. *Environ Pollut.* 2014;184:161–9. <https://doi.org/10.1016/j.envpol.2013.07.027>.
8. Mathalon A, Hill P. Microplastic fibers in the intertidal ecosystem surrounding Halifax Harbor, Nova Scotia. *Mar Pollut Bull.* 2014;81(1):69–79. <https://doi.org/10.1016/j.marpolbul.2014.02.018>.
9. Cole M, Webb H, Lindeque PK, Fileman ES, Halsband C, Galloway TS. Isolation of microplastics in biota-rich seawater samples and marine organisms. *Sci Rep.* 2014;4(1). <https://doi.org/10.1038/srep04528>.
10. Claessens M, Cauwenberghe LV, Vandegehuchte MB, Janssen CR. New techniques for the detection of microplastics in sediments and field collected organisms. *Mar Pollut Bull.* 2013;70(1–2):227–33. <https://doi.org/10.1016/j.marpolbul.2013.03.009>.
11. Karami A, Golieskardi A, Choo CK, Romano N, Ho YB, Salamatinia B. A high-performance protocol for extraction of microplastics in fish. *Sci Total Environ.* 2017;578:485–94. <https://doi.org/10.1016/j.scitotenv.2016.10.213>.
12. Grbic J, Nguyen B, Guo E, You JB, Sinton D, Rochman CM. Magnetic extraction of microplastics from environmental samples. *Environ Sci Technol Lett.* 2019;6(2):68–72. <https://doi.org/10.1021/acs.estlett.8b00671>.
13. Thiele CJ, Hudson MD, Russell AE. Evaluation of existing methods to extract microplastics from bivalve tissue: adapted KOH digestion protocol improves filtration at single-digit pore size. *Mar Pollut Bull.* 2019;142:384–93. <https://doi.org/10.1016/j.marpolbul.2019.03.003>.
14. Pfeiffer F, Fischer EK. Various digestion protocols within microplastic sample processing evaluating the resistance of different synthetic polymers and the efficiency of biogenic organic matter destruction. *Front Environ Sci.* 2020;8. <https://doi.org/10.3389/fenvs.2020.572424>.
15. Lusher AL, Welden NA, Sobral P, Cole M. Sampling, isolating and identifying microplastics ingested by fish and invertebrates. *Anal Methods.* 2017;9(9):1346–60. <https://doi.org/10.1039/c6ay02415g>.
16. Vandermeersch G, Cauwenberghe LV, Janssen CR, Marques A, Granby K, Fait G, et al. A critical view on microplastic quantification in aquatic organisms. *Environ Res.* 2015;143(Pt B):46–55. <https://doi.org/10.1016/j.envres.2015.07.016>.
17. Blasing M, Amelung W. Plastics in soil: analytical methods and possible sources. *Sci Total Environ.* 2018;612:422–35. <https://doi.org/10.1016/j.scitotenv.2017.08.086>.
18. Quinn B, Murphy F, Ewins C. Validation of density separation for the rapid recovery of microplastics from sediment. *Anal Methods.* 2017;9(9):1491–8. <https://doi.org/10.1039/c6ay02542k>.
19. Elert AM, Becker R, Duemichen E, Eisentraut P, Falkenhagen J, Sturm H, et al. Comparison of different methods for MP detection: what can we learn from them, and why asking the right question before measurements matters? *Environ Pollut.* 2017;231(Pt 2):1256–64. <https://doi.org/10.1016/j.envpol.2017.08.074>.

20. K  ppler A, Fischer D, Oberbeckmann S, Schernewski G, Labrenz M, Eichhorn K-J, et al. Analysis of environmental microplastics by vibrational microspectroscopy: FTIR, Raman or both? *Anal Bioanal Chem*. 2016;408(29): 8377–91. <https://doi.org/10.1007/s00216-016-9956-3>.
21. Fischer M, Scholz-B  ttcher BM. Microplastics analysis in environmental samples recent pyrolysis-gas chromatography-mass spectrometry method improvements to increase the reliability of mass-related data. *Anal Methods*. 2019;11(18):2489–97. <https://doi.org/10.1039/c9ay00600a>.
22. Zobkov MB, Esiukova EE. Evaluation of the Munich plastic sediment separator efficiency in extraction of microplastics from natural marine bottom sediments. *Limnol Oceanogr Methods*. 2017;15(11):967–78. <https://doi.org/10.1002/lom3.10217>.
23. Enders K, Lenz R, Stedmon CA, Nielsen TG. Abundance, size and polymer composition of marine microplastics $\geq 10 \mu\text{m}$ in the Atlantic Ocean and their modelled vertical distribution. *Mar Pollut Bull*. 2015;100:70–81. <https://doi.org/10.1016/j.marpolbul.2015.09.027>.
24. L  der MGJ, Gerdts G. Methodology Used for the Detection and Identification of Microplastics—A Critical Appraisal. In: Bergmann M, Gutow L, Klages M. (eds) *Marine Anthropogenic Litter*. Cham: Springer; 2015. https://doi.org/10.1007/978-3-319-16510-3_8.
25. Hurley RR, Lusher AL, Olsen M, Nizzetto L. Validation of a method for extracting microplastics from complex, organic-rich, environmental matrices. *Environ Sci Technol*. 2018;52(13):7409–17. <https://doi.org/10.1021/acs.est.8b01517>.
26. Budimir S, Set  l   O, Lehtiniemi M. Effective and easy to use extraction method shows low numbers of microplastics in offshore planktivorous fish from the northern Baltic Sea. *Mar Pollut Bull*. 2018;127:586–92. <https://doi.org/10.1016/j.marpolbul.2017.12.054>.
27. Julienne F, Delorme N, Lagarde F. From macroplastics to microplastics: role of water in the fragmentation of polyethylene. *Chemosphere*. 2019;236: 124409. <https://doi.org/10.1016/j.chemosphere.2019.124409>.
28. Allegra G, Famulari A. Chain statistics in polyethylene crystallization. *Polymer*. 2009;50(8):1819–29. <https://doi.org/10.1016/j.polymer.2009.01.063>.
29. Julienne F, Lagarde F, Delorme N. Influence of the crystalline structure on the fragmentation of weathered polyolefines. *Polym Degrad Stabil*. 2019; 170:109012. <https://doi.org/10.1016/j.polymdegradstab.2019.109012>.
30. Ober CK, M  llen K. Introduction applications of polymers. In: Matyjaszewski K, M  ller M. (eds) *Polymer science: a comprehensive reference*; Elsevier; 2012. p. 1–8. <https://doi.org/10.1016/B978-0-444-53349-4.00199-0>.
31. Enders K, Lenz R, do Sul JAI, Tagg AS, Labrenz M. When every particle matters: a QuEChERS approach to extract microplastics from environmental samples. *MethodsX*. 2020;7:100784. <https://doi.org/10.1016/j.mex.2020.100784>.
32. Wang Z, Taylor SE, Sharma P, Flury M. Poor extraction efficiencies of polystyrene nano- and microplastics from biosolids and soil. *PLoS One*. 2018;13(11):e0208009. <https://doi.org/10.1371/journal.pone.0208009>.
33. Lares M, Ncibi MC, Sillanp    M, Sillanp    M. Intercomparison study on commonly used methods to determine microplastics in wastewater and sludge samples. *Environ Sci Pollut R*. 2019;26(12):12109–22. <https://doi.org/10.1007/s11356-019-04584-6>.
34. Lenz R, Enders K, Fischer F, Brandt J, Fischer D, Labrenz M. Raman and FTIR spectra used in: Lenz et al. 2021, "Measuring impacts of microplastic treatments via image recognition on immobilised particles below 100 μm "; 2021. <https://doi.org/10.5281/zenodo.4568683>.
35. Lenz R, Enders K, Fischer F, Brandt J, Fischer D, Labrenz M. ImmobileParticles_MatchAndAnalyse: Python code used for analysis of image data in Lenz et al. 2021, "Measuring impacts of microplastic treatments via image recognition on immobilised particles below 100 μm "; 2021. <https://doi.org/10.5281/zenodo.4592319>.
36. VanderPlas J, Granger B, Heer J, Moritz D, Wongsuphasawat K, Satyanarayan A, et al. Altair: interactive statistical visualizations for Python. *J OSS*. 2018; 3(32):1057. <https://doi.org/10.21105/joss.01057>.
37. Satyanarayan A, Moritz D, Wongsuphasawat K, Heer J. Vega-lite: a grammar of interactive graphics. *IEEE Trans Visual Comp Graphics (Proc InfoVis)*. 2017; 23(1):341–50. <https://doi.org/10.1109/tvcg.2016.2599030>.
38. The pandas development team. Pandas-dev/pandas: pandas; 2020. <https://doi.org/10.5281/zenodo.3509134>.
39. McKinney W. Data structures for statistical computing in Python. In: van der WS, Jarrod M, editors. *Proceedings of the 9th Python in Science Conference*; 2010. p. 56–61.
40. Seabold S, Perktold J. Statsmodels: econometric and statistical modeling with Python. In: *9th python in science conference*; 2010.
41. Bradski G. The OpenCV library. *Dr Dobb's J Software Tools*. 2000;25:120–5.
42. Van Der WS, Sch  nberger JL, Nunez-Iglesias J, Boulogne F, Warner JD, Yager N, et al. scikit-image: Image processing in Python. *PeerJ*. 2014;2:e453. <https://doi.org/10.7717/peerj.453>.
43. Canny J. A computational approach to edge detection. *IEEE T Pattern Anal*. 1986;PAMI-8(6):679–98. <https://doi.org/10.1109/tpami.1986.4767851>.
44. Otsu N. A threshold selection method from gray-level histograms. *IEEE Trans Syst Man Cybern*. 1979;9(1):62–6. <https://doi.org/10.1109/tsmc.1979.4310076>.
45. Statsmodels Contributors. 2021. Statsmodels.org. <https://www.statsmodels.org/stable/glm.html>. Accessed 29 Jan 2021.
46. Green PJ. Iteratively reweighted least squares for maximum likelihood estimation, and some robust and resistant alternatives. *J R Stat Soc Ser B Methodol*. 1984;46(2):149–70. <https://doi.org/10.1111/j.2517-6161.1984.tb01288.x>.
47. Lenz R, Enders K, Stedmon CA, Mackenzie DMA, Nielsen TG. A critical assessment of visual identification of marine microplastic using Raman spectroscopy for analysis improvement. *Mar Pollut Bull*. 2015;100(1):82–91. <https://doi.org/10.1016/j.marpolbul.2015.09.026>.
48. Zouboulis E, Renuch D, Grimsditch M. Advantages of ultraviolet Raman scattering for high temperature investigations. *Appl Phys Lett*. 1998;72(1):1–3. <https://doi.org/10.1063/1.121437>.
49. Butler HJ, Ashton L, Bird B, Cinque G, Curtis K, Dorney J, et al. Using Raman spectroscopy to characterize biological materials. *Nat Protoc*. 2016;11(4): 664–87. <https://doi.org/10.1038/nprot.2016.036>.
50. Imhof HK, Laforsch C, Wiesheu AC, Schmid J, Anger PM, Niessner R, et al. Pigments and plastic in limnetic ecosystems: a qualitative and quantitative study on microparticles of different size classes. *Water Res*. 2016;98:64–74. <https://doi.org/10.1016/j.watres.2016.03.015>.
51. Pielh S, Hauk R, Robbe E, Richter B, Kachholz F, Schilling J, et al. Combined approaches to predict microplastic emissions within an urbanized estuary (Warnow, southwestern Baltic Sea). *Front Environ Sci*. 2021;9. <https://doi.org/10.3389/fenvs.2021.616765>.
52. Lenz R, Enders K, Fischer F, Brandt J, Fischer D, Labrenz M. Interactive figure for exploration and analysis of the quantitative image data set in Lenz et al. 2021, "Measuring impacts of microplastic treatments via image recognition on immobilised particles below 100 μm "; 2021. <https://doi.org/10.5281/zenodo.4568524>.
53. de Sousa Menezes M, Queiroz EC, Soares PV, Faria-e-Silva AL, Soares CJ, Martins LRM. Fiber post etching with hydrogen peroxide: effect of concentration and application time. *J Endod*. 2011;37(3):398–402. <https://doi.org/10.1016/j.joen.2010.11.037>.
54. Navarro CA, Kedzie EA, Ma Y, Michael KH, Nutt SR, Williams TJ. Mechanism and catalysis of oxidative degradation of fiber-reinforced epoxy composites. *Top Catal*. 2018;61(7–8):704–9. <https://doi.org/10.1007/s11244-018-0917-2>.
55. Lenz R, Enders K, Fischer F, Brandt J, Fischer D, Labrenz M. DIC microscopy images used in: Lenz et al. 2021, "Measuring impacts of microplastic treatments via image recognition on immobilised particles below 100 μm "; 2021. <https://doi.org/10.5281/zenodo.4568488>.
56. Valsesia A, Quarato M, Ponti J, Fumagalli F, Gilliland D, Colpo P. Combining microcavity size selection with Raman microscopy for the characterization of nanoplastics in complex matrices. *Sci Rep*. 2021;11(1):362. <https://doi.org/10.1038/s41598-020-79714-z>.
57. Al-Azzawi MSM, Kefer S, Wei  er J, Reichel J, Schwaller C, Glas K, et al. Validation of sample preparation methods for microplastic analysis in wastewater matrices reproducibility and standardization. *Water*. 2020;12(9): 2445. <https://doi.org/10.3390/w12092445>.

Publisher's Note

Springer Nature remains neutral with regard to jurisdictional claims in published maps and institutional affiliations.